

On the reliability of analytical models to predict solute transport

C. Cherubini et al.

This discussion paper is/has been under review for the journal Hydrology and Earth System Sciences (HESS). Please refer to the corresponding final paper in HESS if available.

On the reliability of analytical models to predict solute transport in a fracture network

C. Cherubini¹, C. I. Giasi², and N. Pastore²

¹HydRISE, Institut Polytechnique LaSalle Beauvais, 19 rue Pierre Waguët, 60026 Beauvais Cedex, France

²Polytechnical University of Bari, Bari, Italy

Received: 8 November 2013 – Accepted: 21 November 2013 – Published: 6 December 2013

Correspondence to: C. Cherubini (claudia.cherubini@lasalle-beauvais.fr)

Published by Copernicus Publications on behalf of the European Geosciences Union.

Title Page

Abstract

Introduction

Conclusions

References

Tables

Figures

⏪

⏩

◀

▶

Back

Close

Full Screen / Esc

Printer-friendly Version

Interactive Discussion

Abstract

In hydrogeology, the application of reliable tracer transport model approaches is a key issue to derive the hydrodynamic properties of aquifers.

Laboratory and field-scale tracer dispersion breakthrough curves (BTC) in fractured media are notorious for exhibiting early time arrivals and late-time tailing that are not captured by the classical advection–dispersion equation (ADE). These “non-Fickian” features are proved to be better explained by a mobile–immobile (MIM) approach. In this conceptualization the fractured rock system is schematized as a continuous medium in which the liquid phase is separated into flowing and stagnant regions.

The present study compares the performances and reliabilities of classical Mobile–Immobile Model (MIM) and the Explicit Network Model (ENM) that takes expressly into account the network geometry for describing tracer transport behavior in a fractured sample at bench scale. Though ENM shows better fitting results than MIM, the latter remains still valid as it proves to describe the observed curves quite well.

The results show that the presence of nonlinear flow plays an important role in the behaviour of solute transport. Firstly the distribution of solute according to different pathways is not constant but it is related to the flow rate. Secondly nonlinear flow influences advection, in that it leads to a delay in solute transport respect to the linear flow assumption. Whereas nonlinear flow does not show to be related with dispersion. However the interpretation with the ENM model shows a weak transitional regime from geometrical dispersion to Taylor dispersion for high flow rates. The experimental results show that in the study case the geometrical dispersion dominates the Taylor dispersion. Incorporating the description of the flowpaths in the analytical modeling has proved to better fit the curves and to give a more robust interpretation of the solute transport.

HESSD

10, 14905–14948, 2013

On the reliability of analytical models to predict solute transport

C. Cherubini et al.

[Title Page](#)

[Abstract](#)

[Introduction](#)

[Conclusions](#)

[References](#)

[Tables](#)

[Figures](#)

[⏪](#)

[⏩](#)

[◀](#)

[▶](#)

[Back](#)

[Close](#)

[Full Screen / Esc](#)

[Printer-friendly Version](#)

[Interactive Discussion](#)

1 Introduction

In fractured rock formations, the rock mass hydraulic behavior is controlled by fractures. In such aquifers, open and well-connected fractures constitute high permeability pathways and are orders of magnitude more permeable than the rock matrix (Bear and Berkowitz, 1987; Berkowitz, 2002; Bodin et al., 2003; Cherubini, 2008; Cherubini and Pastore, 2011; Geiger et al., 2012; Neuman, 2005).

In most studies examining hydrodynamic processes in fractured media, it is assumed that flow is described by Darcy's law, which expresses a linear relationship between pressure gradient and flow rate (Cherubini and Pastore, 2010). Darcy's law has been demonstrated to be valid at low flow regimes ($Re < 1$). For $Re > 1$ a nonlinear flow behavior is likely to occur.

But in real rock fractures, microscopic inertial phenomena can cause an extra macroscopic hydraulic loss (Kløv, 2000) which deviates flow from the linear relationship among pressure drop and flow rate.

To experimentally investigate fluid flow regimes through deformable rock fractures, Zhang and Nemcik (2013) carried out flow tests through both mated and non-mated sandstone fractures in triaxial cell. For water flow through mated fractures, the experimental data confirmed the validity of linear Darcy's law at low velocity. For larger water flow through non-mated fractures, the relationship between pressure gradient and volumetric flow rate revealed that the Forchheimer equation offers a good description for this particular flow process. The obtained experimental data show that Izbash's law can also provide an excellent description for nonlinear flow. They concluded that further work was needed to study the dependency of the two coefficients on flow velocity.

In fracture networks heterogeneity intervenes even in solute transport: due to the variable aperture and heterogeneities of the fracture surfaces the fluid flow will seek out preferential paths (Gylling et al., 1995) through which solutes are transported.

Generally the geometry of fracture network is not well known and the study of solute transport behavior is based on multiple domain theory according to which the fractured

HESSD

10, 14905–14948, 2013

On the reliability of analytical models to predict solute transport

C. Cherubini et al.

[Title Page](#)

[Abstract](#)

[Introduction](#)

[Conclusions](#)

[References](#)

[Tables](#)

[Figures](#)

[⏪](#)

[⏩](#)

[◀](#)

[▶](#)

[Back](#)

[Close](#)

[Full Screen / Esc](#)

[Printer-friendly Version](#)

[Interactive Discussion](#)



medium is separated in two distinct domains: high velocity zones such as the network of connected fractures (mobile domain) where solute transport occurs predominantly by advection, and lower velocity zones such as secondary pathways, stagnation zones (almost-immobile domain), such as the rock matrix.

5 Therefore in the fracture network different pathways can be identified through which solute is generally distributed in function of the energy spent by solute particles to cross the path. In this context the presence of nonlinear flow plays an important role in the distribution of the solutes according to the different pathways. In fact the energy spent to cross the path is proportional to the resistance to flow associated to the single
10 pathway, which in nonlinear flow regime is not constant but depends on the flow rate.

This means that changing boundary conditions the resistance to flow varies and as a consequence the distribution of solute in the main and secondary pathways also changes giving rise to a different behaviour of solute transport. Moreover, the presence of steep concentration gradients between fractures and matrix causes local disequilibrium in solute concentration which gives rise to dominantly diffusive exchange between
15 fracture and matrix. This explains the non-Fickian nature of transport, which is characterized by breakthrough curves with early first arrival and long tails.

Quantifying solute transport in fractured media has become a very challenging research topic in hydrogeology over the last three decades (Nowamooz et al., 2013).

20 Tracer tests are commonly conducted in such aquifers to estimate transport parameters such as effective porosity and dispersivity, to characterize subsurface heterogeneity, and to directly delineate flow paths. Testing involves injecting a tracer into the underground formation through an injection well, and then monitoring the tracer concentrations as a function of location and/or time at the surrounding observation well
25 (breakthrough curve).

Transport parameters such as porosity and dispersion coefficient are estimated by fitting appropriate tracer transport models to the breakthrough data.

In this context, analytical models are frequently employed, especially for analyzing tests obtained under controlled conditions, because they involve a small number of

HESSD

10, 14905–14948, 2013

On the reliability of analytical models to predict solute transport

C. Cherubini et al.

Title Page

Abstract

Introduction

Conclusions

References

Tables

Figures

⏪

⏩

◀

▶

Back

Close

Full Screen / Esc

Printer-friendly Version

Interactive Discussion

parameters and provide physical insights into solute transport processes (Liu et al., 2012).

The advection–dispersion equation (ADE) has been traditionally applied to model tracer transport in fractures. However extensive evidence has shown that there exist two main features that cannot be explained by the ADE: the early first arrival and the long tail of the observed BTCs curves (Neretnieks et al., 1982; Becker and Shapiro, 2000; Jiménez-Hornero et al., 2005; Bauguet and Fourar, 2008).

Several other models have been used to fit the anomalous BTCs obtained in laboratory tracer tests carried out in single fractures. Among those, the Mobile–Immobile (MIM) model (van Genuchten and Wierenga, 1976), which recognizes the existence of mobile and immobile domains for transport, has showed to provide better fits of BTC curves (Gao et al., 2009; Schumer et al., 2003; Feehley et al., 2010).

In the well-controlled laboratory tracer tests carried out by Qian et al. (2011) a mobile–immobile (MIM) model proved to fit both peak and tails of the observed BTCs better than the classical ADE model.

Another powerful method to describe non-Fickian transport in fractured media is the continuous time random walk (CTRW) approach (Berkowitz et al., 2006) which is based on the conceptual picture of tracer particles undergoing a series of transitions of length s and time t .

Together with a master equation conserving solute mass, the random walk is developed into a transport equation in partial differential equation form. The CTRW has been successfully applied for describing non-Fickian transport in single fractures (Berkowitz et al., 2001; Jiménez-Hornero et al., 2005).

Bauguet and Fourar (2008) investigated non-Fickian transport in a transparent replica of a real single fracture. They employed three different models including ADE, CTRW, and a stratified model to interpret the tracer experiments.

As expected, the solution derived from the ADE equation appears to be unable to model long-time tailing behavior. On the other hand, the CTRW and the stratified model

HESSD

10, 14905–14948, 2013

On the reliability of analytical models to predict solute transport

C. Cherubini et al.

Title Page

Abstract

Introduction

Conclusions

References

Tables

Figures

⏪

⏩

◀

▶

Back

Close

Full Screen / Esc

Printer-friendly Version

Interactive Discussion

were able to describe non-Fickian dispersion. The parameters defined by these models are correlated to the heterogeneities of the fracture.

Nowamooz et al. (2013) carried out experimental investigation and modeling analysis of tracer transport in transparent replicas of two Vosges sandstone natural fractures.

The obtained breakthrough curves were then interpreted using a stratified medium model that incorporates a single parameter permeability distribution to account for fracture heterogeneity, together with a CTRW model, as well as the classical ADE model.

The results indicated that the classical ADE is not appropriate for modeling early first arrival and long-time tailing. In contrast, the stratified model provides generally satisfactory matches to the data (even though it cannot explain the long-time tailing adequately) while the CTRW model captures the full evolution of the long tailing displayed by the breakthrough curves.

Qian et al. (2011) experimentally studied solute transport in a single fracture (SF) under non-Darcian flow condition which was found to closely follow the Forchheimer equation.

They also investigated on the influence of the velocity contrast between the fracture wall and the plane of symmetry on the dispersion process, which was called “boundary layer dispersion” by Koch and Brady (1985).

They affirmed that this phenomenon had to be considered if the thickness of the boundary layer was greater than the roughness of the fracture. On the other hand, if the thickness of the boundary layer was smaller than the roughness of the fractures, the recirculation zones inside the roughness cavities rather than the boundary layer would be more relevant for the dispersion process, thus the hold-up dispersion would become important. Since smooth parallel planes were used for constructing the SF in their experiment, the fracture roughness and the hold-up dispersion were negligible.

Bodin et al. (2007) developed the SOLFRAC program, which performs fast simulations of solute transport in complex 2-D fracture networks using the Time Domain Random Walk (TDRW) approach (Delay and Bodin, 2001) that makes use of a pipe network approximation. The code accounts for advection and hydrodynamic dispersion

HESSD

10, 14905–14948, 2013

On the reliability of analytical models to predict solute transport

C. Cherubini et al.

[Title Page](#)

[Abstract](#)

[Introduction](#)

[Conclusions](#)

[References](#)

[Tables](#)

[Figures](#)

[⏪](#)

[⏩](#)

[◀](#)

[▶](#)

[Back](#)

[Close](#)

[Full Screen / Esc](#)

[Printer-friendly Version](#)

[Interactive Discussion](#)



in channels, matrix diffusion, diffusion into stagnant zones within the fracture planes, mass sharing at fracture intersections, and other mechanisms such as sorption reactions and radioactive decay. Comparisons between numerical results and analytical breakthrough curves for synthetic test problems have proven the accuracy of the model.

5 Zafarani and Detwiler (2013) presented an alternate approach for efficiently simulating transport through fracture intersections.

Rather than solving the two-dimensional Stokes equations, the model relies upon a simplified velocity distribution within the fracture intersection, assuming local parabolic velocity profiles within fractures entering and exiting the fracture intersection. Therefore, the solution of the two-dimensional Stokes equations is unnecessary, which greatly reduces the computational complexity. The use of a time-domain approach to route particles through the fracture intersection in a single step further reduces the number of required computations. The model accurately reproduces mixing ratios predicted by high-resolution benchmark simulations.

15 Starting from previous studies (Cherubini et al., 2012, 2013a), in order to give a physical interpretation of the flow and transport behavior, in this work the experimental results of flow and transport tests in a fractured block at bench scale are interpreted by means of two conceptual models: the single rate mobile-immobile model (MIM) and the Explicit Network Model (ENM). Differently from the former, the latter expressly takes the fracture network geometry into account.

The MIM approach is applied successfully in a broad variety of environmental contexts such as rivers and streams with hypoxic zone exchange, subsurface flow and transport in unsaturated and saturated heterogeneous media, reactive solute transport etc.

25 When applied to fractured media, the MIM approach does not explicitly take the fracture network geometry into account, but it conceptualizes the shape of fractures as one dimensional continuous media in which the liquid phase is separated into flowing and stagnant regions. The convective dispersive transport is restricted to the flowing region, and the solute exchange is described as a first-order process.

On the reliability of analytical models to predict solute transport

C. Cherubini et al.

Title Page

Abstract

Introduction

Conclusions

References

Tables

Figures

⏪

⏩

◀

▶

Back

Close

Full Screen / Esc

Printer-friendly Version

Interactive Discussion



On the reliability of analytical models to predict solute transport

C. Cherubini et al.

Title Page

Abstract

Introduction

Conclusions

References

Tables

Figures

⏪

⏩

◀

▶

Back

Close

Full Screen / Esc

Printer-friendly Version

Interactive Discussion

Where t (T) is the time, x (L) is the spatial coordinate along the direction of the flow, c_m and c_{im} (ML^{-3}) are the cross-sectional averaged solute concentrations respectively in the mobile and immobile domain, v (LT^{-1}) is the average flow velocity and D (L^2T^{-1}) is the dispersion coefficient, α (T^{-1}) is the mass exchange coefficient, β [-] is the mobile water fraction. For a non-reactive solute β is equivalent to the ratio between the

The solution of system Eq. (7) describing one-dimensional (1-D) non-reactive solute transport in an infinite domain for instantaneous pulse of solute injected at time zero at the origin is given by (Goltz and Roberts, 1986):

$$c_1(x, t) = e^{-\alpha t} c_0(x, t) + \alpha \int_0^t H(t, \tau) c_0(x, \tau) d\tau. \quad (8)$$

c_0 represents the analytical solution for the classical advection–dispersion equation (Crank, 1956):

$$c_0(x, t) = \frac{M_0}{\omega \sqrt{\pi D t}} e^{-\frac{(x-vt)^2}{4Dt}} \quad (9)$$

where M_0 (M) is the mass of the tracer injected instantaneously at time zero at the origin of the domain. The term $H(t, \tau)$ presents the following expression:

$$H(t, \tau) = e^{-\frac{\alpha}{\beta}(t-\tau) - \alpha\tau} \frac{\tau I_1\left(\frac{2\alpha}{\beta} \sqrt{\beta(t-\tau)\tau}\right)}{\sqrt{\beta(t-\tau)\tau}} \quad (10)$$

where I_1 represents the modified Bessel function of order 1.

In order to fit the BTCs curves the length of 1-D domain does not need to be known. The parameters v and D are normalized by dividing them by L and L^2 respectively. In this way a unit length of 1-D domain can be assumed.

The ENM is defined by six parameters regarding each single fracture (a , b , P_Q , ω , α_L and P_c).

3 Material and methods

3.1 Experimental setup

5 The experiments have been performed on a limestone block with parallelepiped shape (0.6 m \times 0.4 m \times 0.08 m) recovered from the “Calcare di Altamura” formation which is located in Apulia region in southeastern Italy (Cherubini et al., 2012).

The experimental setup is detailed in Cherubini et al. (2012, 2013a) and its schematic diagram is shown in Fig. 1.

10 3.1.1 Flow tests

The analysis of flow dynamics through the selected path (Fig. 2) regards the observation of water flow from the upstream tank to the flow cell with a circular cross-section of 0.1963 m² and 1.28 \times 10⁻⁴ m² respectively.

15 Initially at time t_0 , the valves “a” and “b” are closed and the hydrostatic head in the flow cell is equal to h_0 . The experiment begins with the opening of the valve “a” which is reclosed when the hydraulic head in the flow cell is equal to h_1 . Finally the hydraulic head in the flow cell is reported to h_0 through the opening of the valve “b”. The experiment procedure is repeated changing the hydraulic head of the upstream tank h_c . The time $\Delta t = (t_1 - t_0)$ required to fill the flow cell from h_0 to h_1 has been registered.

20 Given that the capacity of the upstream tank is much higher than that of the flow cell it is reasonable to assume that during the experiments the level of the upstream tank (h_c) remains constant. Under this hypothesis the flow inside the system is governed by the equation:

On the reliability of analytical models to predict solute transport

C. Cherubini et al.

Title Page

Abstract

Introduction

Conclusions

References

Tables

Figures

⏪

⏩

◀

▶

Back

Close

Full Screen / Esc

Printer-friendly Version

Interactive Discussion



$$S_1 \frac{dh}{dt} = \Gamma(\Delta h)(h_c - h) \quad (20)$$

where S_1 (L²) and h (L) are respectively the section area and the hydraulic head of the flow cell; h_c (L) is the hydraulic head of upstream tank, $\Gamma(\Delta h)$ represents the hydraulic conductance term representative of both hydraulic circuit and the selected path.

5 The average flow rate \bar{Q} can be estimated by means of the volumetric method:

$$\bar{Q} = \frac{S_1}{t_1 - t_0} (h_1 - h_0) \quad (21)$$

whereas the average hydraulic head difference $\overline{\Delta h}$ is given by:

$$\overline{\Delta h} = h_c - \frac{h_0 + h_1}{2}. \quad (22)$$

10 In correspondence of the average flow rate and head difference is it possible to evaluate the average hydraulic conductance as:

$$\bar{\Gamma}(\Delta h) = \frac{S_1}{t_1 - t_0} \ln \left(\frac{h_0 - h_c}{h_1 - h_c} \right). \quad (23)$$

The inverse of $\bar{\Gamma}(\Delta h)$ represents the average resistance to flow $\bar{R}(\bar{Q})$.

3.1.2 Tracer tests

15 The study of solute transport dynamics through the selected path has been carried out by means of a tracer test using sodium chloride. Initially a hydraulic head difference between the upstream tank and downstream tank is imposed. At $t = 0$ the valve “a” is closed and the hydrostatic head inside the block is equal to the downstream tank.

Title Page

Abstract

Introduction

Conclusions

References

Tables

Figures

⏪

⏩

◀

▶

Back

Close

Full Screen / Esc

Printer-friendly Version

Interactive Discussion



At $t = 10$ s the valve “a” is opened while at time $t = 60$ s a mass of solute equal to 5×10^{-4} kg is injected into the inlet port through a syringe. The source release time (1 s) is very small therefore the instantaneous source assumption can be considered valid.

In correspondence of the flow cell in which the multi-parametric probe is located it is possible to measure the tracer breakthrough curve and the hydraulic head; in the meanwhile the flow rate entering the system is measured by means of an ultrasonic velocimeter. For different flow rates a BTC curve can be recorded at the outlet port.

Time moment analysis has been applied in order to characterize the BTC curves in terms of mean breakthrough time, degree of spread and asymmetry.

The mean residence time t_m is given by:

$$t_m = \frac{\int_0^{\infty} t^n c(t) dt}{\int_0^{\infty} c(t) dt}. \quad (24)$$

The n th normalized central moment of distribution of solute concentration vs. time is defined as:

$$\mu_n = \frac{\int_0^{\infty} [t - t_m]^n c(t) dt}{\int_0^{\infty} c(t) dt}. \quad (25)$$

The second moment μ_2 represents the degree of spread relative to t_m . whereas the degree of asymmetry measured by the skewness coefficient is defined as:

$$S = \mu_3 / \mu_2^{3/2}. \quad (26)$$

On the reliability of analytical models to predict solute transport

C. Cherubini et al.

Title Page	
Abstract	Introduction
Conclusions	References
Tables	Figures
⏪	⏩
◀	▶
Back	Close
Full Screen / Esc	
Printer-friendly Version	
Interactive Discussion	



4 Discussion

4.1 Estimation of flow model parameters

The flow field in each single fracture of the network can be solved in analytical way by means of Kirchhoff laws. In Fig. 2 is represented the 2-D-pipe network conceptualization.

The resistance to flow of each single j fracture is described by the Eq. (12). The Forchheimer parameters are assumed constant for the whole fracture network.

The application of the Kirchhoff's first law at the node 3 can be written as:

$$Q_0 - Q_1 - Q_2 = 0 \quad (27)$$

whereas the application of the Kirchhoff's second law at the loop 3–4–5–6 can be written as:

$$R_6(Q_1)Q_1 - (R_3(Q_2) + R_4(Q_2) + R_5(Q_2))Q_2 = 0. \quad (28)$$

Substituting Eq. (28) into Eq. (29) the iterative equation of flow rate Q_1 can be obtained:

$$Q_1^{k+1} = Q_0 \left[\frac{R_3(Q_0 - Q_1^k) + R_4(Q_0 - Q_1^k) + R_5(Q_0 - Q_1^k)}{R_3(Q_0 - Q_1^k) + R_4(Q_0 - Q_1^k) + R_5(Q_0 - Q_1^k) + R_6(Q_1^k)} \right]. \quad (29)$$

The Forchheimer parameters representative of whole fracture network can be derived matching the average resistance to flow derived experimentally with the resistance to flow evaluated for the whole network:

$$\bar{R}(\bar{Q}) = R_1(Q_0) + R_2(Q_0) + \left(\frac{1}{R_6(Q_1)} + \frac{1}{R_3(Q_2) + R_4(Q_2) + R_5(Q_2)} \right)^{-1} + R_7(Q_0) + R_8(Q_0) + R_9(Q_0). \quad (30)$$

HESSD

10, 14905–14948, 2013

On the reliability of analytical models to predict solute transport

C. Cherubini et al.

Title Page

Abstract

Introduction

Conclusions

References

Tables

Figures

⏪

⏩

◀

▶

Back

Close

Full Screen / Esc

Printer-friendly Version

Interactive Discussion



Figure 3 shows the fitting of observed resistance to flow determined by the inverse of Eq. (24) and the theoretical resistance to flow (Eq. 31). The linear and nonlinear terms of Forchheimer model in Eq. (12) have been estimated and they are respectively equal to $a = 7.345 \times 10^4 \text{ s m}^{-3}$ and $b = 11.65 \times 10^9 \text{ s}^2 \text{ m}^{-6}$. It is evident that the 2-D-pipe network model closely matches the experimental results ($r^2 = 0.9913$). Flow characteristics can be studied through the analysis of Forchheimer number F_o which represents the ratio of nonlinear to linear hydraulic gradient contribution:

$$F_o = \frac{bQ}{a}. \quad (31)$$

Inertial forces dominate over viscous ones at the critical Forchheimer number ($F_o = 1$) corresponding in our case to a flow rate equal to $Q_{\text{crit}} = 6.30 \times 10^{-6} \text{ m}^3 \text{ s}^{-1}$, which is coherent with the results obtained in the previous study (Cherubini et al., 2013a).

The term in square brackets in Eq. (30) represents the probability of water distribution P_Q evaluated for the branch 6. Note that it is not constant but it depends on the flow rate crossing the parallel branch. Figure 4 shows P_Q as function of Q_o . The probability of water distribution decreases as the injection flow rate increases. This means that when the injection flow rate increases the resistance to flow of the branch 6 increases faster than the resistance to flow of the branch 3–4–5 and therefore the solute chooses the secondary pathway.

4.2 Fitting of breakthrough curves and interpretation of estimated transport model parameters

Several tests have been conducted in order to observe solute transport behavior varying the injection flow rate in the range $1.20 \times 10^{-6} - 9.34 \times 10^{-6} \text{ m}^3 \text{ s}^{-1}$. For each experimental BTCs the mean travel time t_m and the coefficient of Skewness S have been estimated.

Figure 5 shows t_m as function of Q_o . Travel time decreases more slowly for high flow rates. In particular a change of slope is evident in correspondence of the injection

Title Page

Abstract

Introduction

Conclusions

References

Tables

Figures

⏪

⏩

◀

▶

Back

Close

Full Screen / Esc

Printer-friendly Version

Interactive Discussion

flow rate equal to $4 \times 10^{-6} \text{ m}^3 \text{ s}^{-1}$ (Cherubini et al., 2013a), which evidences a delay of solute transport for high flow rates. Note that this behaviour occurs before Q_{crit} .

The skewness coefficient does not exhibit a trend upon varying the injection flow rate, but its mean value is equal to 2.018. A positive value of skewness indicates that BTCs are asymmetric with early first arrival and long tail. This behavior seems not to be dependent on the presence of the transitional regime.

The measured breakthrough curves for different flow rates have been individually fitted by MIM $(v/L, D/L^2, \alpha, \beta)$ and ENM $(\omega_{\text{eq}}, \alpha_L, P_Q, P_C)$ models.

In particular for the ENM model the parameters ω_{eq} and α_L are representative of all fracture network, whereas the parameter P_Q and P_C are associated only to the parallel branches. For the considered fracture network the Eq. (16) becomes:

$$C_{\text{out}} = \frac{M_0}{Q_0} F^{-1} \left[P_C \cdot F(s_1) \cdot F(s_2) \cdot F(s_6) \cdot F(s_7) \cdot F(s_8) \cdot F(s_9) + (1 - P_C) \cdot F(s_1) \cdot F(s_2) \cdot F(s_3) \cdot F(s_4) \cdot F(s_5) \cdot F(s_7) \cdot F(s_8) \cdot F(s_9) \right]. \quad (32)$$

The velocity and dispersion that characterize the probability density function s are related to the flow rate that crosses each branch by Eqs. (19) and (20). This one is equal to the injection flow rate Q_0 except for branch 6 and branches 3–4–5 for which it is equal to $Q = P_Q Q_0$ and $Q = (1 - P_Q) Q_0$, respectively.

Furthermore three parameter configurations have been tested for the ENM model. The configurations are distinguished on the basis of the number of fitting parameters and assumptions made on P_C and P_Q parameters. The first configuration named ENM2 has two fitting parameters ω_{eq} and α_L . In this configuration P_C is imposed equal to P_Q and is estimated by the flow tests described in previous sections.

The second configuration named ENM3 has three fitting parameters ω_{eq} and α_L and P_C . In this configuration is it still true that P_C is equal to P_Q and both of them are estimated by the interpretation of BTC curves.

In the third configuration named ENM4 all four parameters $(\omega_{\text{eq}}, \alpha_L, P_Q, P_C)$ are estimated through the fitting of BTCs.

HESSD

10, 14905–14948, 2013

On the reliability of analytical models to predict solute transport

C. Cherubini et al.

Title Page

Abstract

Introduction

Conclusions

References

Tables

Figures

⏪

⏩

◀

▶

Back

Close

Full Screen / Esc

Printer-friendly Version

Interactive Discussion



To compare all the considered models, both the determination coefficient (r^2) and the root mean square error (RMSE) were used as criteria to determine the goodness of the fitting, which can be expressed as:

$$r^2 = 1 - \frac{\sum_{i=1}^N (C_{i,o} - C_{i,e})^2}{\sum_{i=1}^N (C_{i,o} - \bar{C}_{i,o})^2} \quad (33)$$

$$RMSE = \sqrt{\frac{1}{N} \sum_{i=1}^N (C_{i,o} - C_{i,e})^2} \quad (34)$$

where N is the number of observations, $C_{i,e}$ is the estimated concentration, $C_{i,o}$ is the observed concentration, $\bar{C}_{i,o}$ represents the mean value of $C_{i,o}$.

Tables 1–4 show the estimated values of parameters, root mean square error RMSE and the determination coefficient r^2 for all the considered models varying the inlet flow rate Q_0 .

Figure 6 shows the fitting results of BTC curves for different injection flow rates.

For higher flow rates (7.07×10^{-6} and $4.80 \times 10^{-6} \text{ m}^3 \text{ s}^{-1}$) the fitting is poorer than for lower flow rates (3.21×10^{-6} and $1.96 \times 10^{-6} \text{ m}^3 \text{ s}^{-1}$). However, all models provide a satisfactory fitting. The ENM4 model provides the highest values of r^2 varying in the range 0.9921–1.000 and the smallest values of RMSE in the range 0.0033–0.0252. This is expected for two reasons. First this model has more fitting parameters than ENM2 and ENM3, thus it is more flexible. Secondly, compared to MIM model, it takes explicitly into account the presence of the secondary path.

The MIM model considers the existence of immobile and mobile domains and a rate-limited mass transfer between these two domains. In the present context this conceptualization can be a weak assumption especially for high flow rates when the importance

HESSD

10, 14905–14948, 2013

On the reliability of analytical models to predict solute transport

C. Cherubini et al.

Title Page

Abstract

Introduction

Conclusions

References

Tables

Figures

⏪

⏩

◀

▶

Back

Close

Full Screen / Esc

Printer-friendly Version

Interactive Discussion

of secondary path increases. However the fitting of BTCs shows that MIM model remains valid as it proves to describe the observed curves quite well.

Although somewhat scattered, the mass transfer coefficient of MIM model tends to increase with pore water velocity. Several authors have observed the variation of the mass-transfer coefficient between mobile and immobile water regions with pore-water velocity (van Genuchten and Wierenga, 1977; Nkedi-Kizza et al., 1984; De Smedt and Wierenga, 1984; De Smedt et al., 1986; Schulin et al., 1987). The increase in α with increasing water velocity is attributed to higher mixing in the mobile phase at high pore water velocities (De Smedt and Wierenga, 1984) or to shorter diffusion path lengths as a result of a decrease in the amount of immobile water (van Genuchten and Wierenga, 1977).

In the study, the increase in α with increasing water velocity is attributable to non-linear flow that enhances the exchange between the main and secondary flow paths. Therefore the mass transfer coefficient increases as the importance of secondary path over the main path increases.

The extent of solute mixing can also be assessed from the analysis of MIM mobile water fraction parameter β . In our study the fraction of mobile water assumes a mean representative value of 0.56 meaning that the 0.56 % of the soil is involved in advective transport. Various authors have observed different behavior of the mobile water fraction parameter β . Gaudet et al. (1977) reported increasing mobile water content with increasing pore water velocity. However, studies have also found that β appears to be constant with varying pore-water velocity (Nkedi-kizza et al., 1983). With the increase of mobile water fraction, the contact areas between the mobile and immobile regions increase, enhancing solute mixing between these two regions (Gao et al., 2009). However, lower β values can be attributed to faster initial movement of the solute as it travels through a decreasing number of faster flow paths. As a result, some authors have related β values to the initial arrival of the solute. In fact, Gaudet et al. (1977) and Selim and Ma (1995) observed that the mobile water fraction parameter affects the time of initial appearance of the solute.

On the reliability of analytical models to predict solute transport

C. Cherubini et al.

Title Page

Abstract

Introduction

Conclusions

References

Tables

Figures

⏪

⏩

◀

▶

Back

Close

Full Screen / Esc

Printer-friendly Version

Interactive Discussion



words varying the injection flow rate the conductance of the main path decreases more rapidly than the conductance of the secondary path.

The BTCs curves determined by transport experiments have been fitted by MIM model (ENM2, ENM3, ENM4) which differ on the basis of the assumptions made on the parameter P_Q and P_C . All models prove a satisfactory fitting. The ENM4 model provides the best fit which is expectable because it has more fitting parameters than ENM2 and ENM3, thus it is more flexible. Second, compared to MIM model, it takes explicitly into account the presence of the secondary path. Furthermore for the ENM model the parameter P_Q decreases more rapidly varying the injection flow rate than the same parameter evaluated by flow tests. The relationship between transport time and exchange time for MIM model and mean travel time for main path and secondary path for the ENM4 model varying the injection flow rate has shown similarity of behaviour: for higher values of flow rate the difference between transport time and exchange time decreases and the secondary path reaches the main path in terms of mean travel time. This analogy between MIM and ENM explains the fact that the mass transfer coefficient is dependent on flow velocity. The mass transfer coefficient increases as the importance of secondary path over the main path increases.

The velocity values evaluated for MIM and ENM model show the same relationship with the injection flow rate. In particular a change of slope is evident in correspondence of the flow rate equal to $4 \times 10^{-6} \text{ m}^3 \text{ s}^{-1}$. This behaviour occurs before the critical flow rate estimated by flow tests equal to $6.3 \times 10^{-6} \text{ m}^3 \text{ s}^{-1}$. Therefore the interpretation of BTCs curves evidences more enhanced nonlinear behavior than flow tests. These results confirm the fact that the presence of transitional flow regime leads to a delay on solute transport with respect to the values that can be obtained under the assumption of a linear flow field (Cherubini et al., 2013a).

As concerns dispersion, a linear trend varying the velocity for both MIM and ENM models has been observed – coherently with the previous results – (Cherubini et al., 2013a), the MIM model underestimating the dispersion respect to ENM4 model.

HESSD

10, 14905–14948, 2013

On the reliability of analytical models to predict solute transport

C. Cherubini et al.

Title Page

Abstract

Introduction

Conclusions

References

Tables

Figures

⏪

⏩

◀

▶

Back

Close

Full Screen / Esc

Printer-friendly Version

Interactive Discussion

On the reliability of analytical models to predict solute transport

C. Cherubini et al.

[Title Page](#)

[Abstract](#)

[Introduction](#)

[Conclusions](#)

[References](#)

[Tables](#)

[Figures](#)

[⏪](#)

[⏩](#)

[◀](#)

[▶](#)

[Back](#)

[Close](#)

[Full Screen / Esc](#)

[Printer-friendly Version](#)

[Interactive Discussion](#)

The dispersivity values obtained for ENM models do not depend on flow velocity but assume a somehow scattered but fluctuating value. Being α_L values constant, geometrical dispersion dominates the mixing processes along the fracture network. Therefore, the presence of a nonlinear flow regime does not prove to exert any influence on dispersion except for high velocities for the ENM model where a weak transitional regime seems to appear. This result demonstrates that for our experiment geometrical dispersion still dominates Taylor dispersion.

Differently from “black-box” one-dimensional models the definition of the network of fracture may allow to better characterize the nonlinear flow behavior and its influence on solute propagation in a fractured medium at bench scale (Cherubini et al., 2013b).

References

- Bauget, F. and Fourar, M.: Non-Fickian dispersion in a single fracture, *J. Contam. Hydrol.*, 100, 137–148, doi:10.1016/j.jconhyd.2008.06.005, 2008.
- Bear, J.: *Dynamics of Fluids in Porous Media*, Elsevier, New York, 1972.
- Bear, J. and Berkowitz, B.: Groundwater flow and pollution in fractured rock aquifers, in: *Developments in Hydraulic Engineering*, vol. 4, edited by: Novak, P., Elsevier Applied Science Publishers Ltd., New York, 175–238, 1987.
- Becker, M. W. and Shapiro, A. M.: Tracer transport in fractured crystalline rock: evidence of nondiffusive breakthrough tailing, *Water Resour. Res.*, 36, 1677–1686, doi:10.1029/2000WR900080, 2000.
- Berkowitz, B.: Characterizing flow and transport in fractured geological media: a review, *Adv. Water Resour.*, 25, 861–884, 2002.
- Berkowitz, B., Cortis, A., Dentz, M., and Scher, H.: Modeling non-Fickian transport in geological formations as a continuous time random walk, *Rev. Geophys.*, 44, RG2003, doi:10.1029/2005RG000178, 2006.
- Bodin, J., Delay, F., and de Marsily, G.: Solute transport in a single fracture with negligible matrix permeability: 1. fundamental mechanisms, *Hydrogeol. J.*, 11, 418–433, 2003.

On the reliability of analytical models to predict solute transport

C. Cherubini et al.

[Title Page](#)[Abstract](#)[Introduction](#)[Conclusions](#)[References](#)[Tables](#)[Figures](#)[⏪](#)[⏩](#)[◀](#)[▶](#)[Back](#)[Close](#)[Full Screen / Esc](#)[Printer-friendly Version](#)[Interactive Discussion](#)

- Bodin, J., Porel, G., Delay, F., Ubertosi, F., Bernard, S., and de Dreuzy, J.: Simulation and analysis of solute transport in 2-D fracture/pipe networks: the SOLFRAC program, *J. Contam. Hydrol.*, 89, 1–28, 2007.
- 5 Cherubini, C.: A modeling approach for the study of contamination in a fractured aquifer, in: *Geotechnical and Geological Engineering*, vol. 26, Springer, the Netherlands, 519–533, 2008.
- Cherubini, C. and Pastore, N.: Modeling contaminant propagation in a fractured and karstic aquifer, *Fresen. Environ. Bull.*, 19, 1788–1794, 2010.
- Cherubini, C. and Pastore, N.: Critical stress scenarios for a coastal aquifer in southeastern Italy, *Nat. Hazards Earth Syst. Sci.*, 11, 1381–1393, doi:10.5194/nhess-11-1381-2011, 2011.
- 10 Cherubini, C., Giasi, C. I., and Pastore, N.: Bench scale laboratory tests to analyze non-linear flow in fractured media, *Hydrol. Earth Syst. Sci.*, 16, 2511–2522, doi:10.5194/hess-16-2511-2012, 2012.
- 15 Cherubini, C., Giasi, C. I., and Pastore, N.: Evidence of non-Darcy flow and non-Fickian transport in fractured media at laboratory scale, *Hydrol. Earth Syst. Sci.*, 17, 2599–2611, doi:10.5194/hess-17-2599-2013, 2013a.
- Cherubini, C., Giasi, C. I., and Pastore, N.: Fluid flow modeling of a coastal fractured karstic aquifer by means of a lumped parameter approach, *Environ. Earth Sci.*, 70, 2055–2060, 2013b.
- 20 Delay, F. and Bodin, J.: Time domain random walk method to simulate transport by advection–dispersion and matrix diffusion in fracture networks, *Geophys. Res. Lett.*, 28, 4051–4054, 2001.
- De Smedt, F. and Wierenga, P. J.: Solute transfer through columns of glass beads, *Water Resour. Res.*, 20, 225–232, 1984.
- 25 Feehley, C. E., Zheng, C., and Molz, F. J.: A dual-domain mass transfer approach for modeling solute transport in heterogeneous aquifers: Application to the Macrodispersion Experiment (MADE) site, *Water Resour. Res.*, 36, 2501–2515, 2010.
- Forchheimer, P.: *Wasserbewegung durch Boden*, *Z. Verein Deut. Ing.*, 45, 1781–1788, 1901.
- 30 Gaudet, J. P., Jégat, H., Vachaud, G., and Wierenga, P. J.: Solute transfer, with exchange between mobile and stagnant water, through unsaturated sand, *Soil Sci. Soc. Am. J.*, 41, 665–671, 1977.

On the reliability of analytical models to predict solute transport

C. Cherubini et al.

[Title Page](#)

[Abstract](#)

[Introduction](#)

[Conclusions](#)

[References](#)

[Tables](#)

[Figures](#)

[⏪](#)

[⏩](#)

[◀](#)

[▶](#)

[Back](#)

[Close](#)

[Full Screen / Esc](#)

[Printer-friendly Version](#)

[Interactive Discussion](#)

Geiger, S., Cortis, A., and Birkholzer, J. T.: Upscaling solute transport in naturally fractured porous media with the continuous time random walk method, *Water Resour. Res.*, 46, doi:10.1029/2010WR009133, 2010.

Gylling, B., Moreno, L., and Neretnieks, I.: Transport of solute in fractured media, based on a channel network model, in: *Proceedings of Groundwater Quality: Remediation and Protection Conference*, edited by: Kovar, K. and Krasny, J., 14–19 May, Prague, 107–113, 1995.

Jiménez-Hornero, F. J., Giráldez, J. V., Laguna, A., and Pachepsky, Y.: Continuous time randomwalks for analyzing the transport of a passive tracer in a single fissure, *Water Resour. Res.*, 41, W04009, doi:10.1029/2004WR003852, 2005.

Kamra, S. K., Lennartz, B., van Genuchten, M. T., and Widmoser, P.: Evaluating non-equilibrium solute transport in small soil columns, *J. Contam. Hydrol.*, 48, 189–212, 2001.

Klov, T.: High-velocity flow in fractures, Dissertation for the partial fulfillment of the requirements for the degree of doktor ingeniør Norwegian University of Science Technology Department of Petroleum Engineering and Applied Geophysics, Trondheim, 2000.

Liu, H. H., Mukhopadhyay, S., Spycher, N., and Kennedy, B. M.: Analytical solutions of tracer transport in fractured rock associated with precipitation-dissolution reactions, *Hydrogeol. J.*, 19, 1151–1160, 2011.

Moutsopoulos, K. N., Papaspyros, I. N. E., and Tsihrintzis, V. A.: Experimental investigation of inertial flow processes in porous media, *J. Hydrol.*, 374, 242–254, 2009.

Mulla, D. J. and Stroock, J. S.: Nitrogen transport processes in soil, in: *Nitrogen in agricultural systems*, edited by: Schepers, J. S. and Raun, W. R., Agron. Monogr. 49, ASA, CSSA, SSSA, Madison, WI, 401–436, 2008.

Neretnieks, I., Eriksen, T., and Tahtinen, P.: Tracer movement in a single fissure in granitic rock: some experimental results and their interpretation, *Water Resour. Res.*, 18, 849–858, doi:10.1029/WR018i004p00849, 1982.

Neuman, S. P.: Trends, prospects and challenges in quantifying flow and transport through fractured rocks, *Hydrogeol. J.*, 13, 124–147, 2005.

Nkedi-Kizza, P., Biggar, J. W., van Genuchten, M. T., Wierenga, P. J., Selim, H. M., Davidson, J. M., and Nielsen, D. R.: Modeling tritium and chloride 36 transport through an aggregated oxisol, *Water Resour. Res.*, 19, 691–700, 1983.

Nowamooz, A., Radilla, R., Fourar, M., and Berkowitz, B.: Non-Fickian Transport in Transparent Replicas of Rough-Walled Rock Fractures Transport in Porous Media July 2013, 98, 651–682, doi:10.1007/s11242-013-0165-7, 2013.

On the reliability of analytical models to predict solute transport

C. Cherubini et al.

Title Page

Abstract

Introduction

Conclusions

References

Tables

Figures

⏪

⏩

◀

▶

Back

Close

Full Screen / Esc

Printer-friendly Version

Interactive Discussion



Qian, J. Z., Chen, Z., Zhan, H. B., and Luo, S. H.: Solute transport in a filled single fracture under non-Darcian flow, *Int. J. Rock Mech. Min.*, 48, 132–140, 2011.

Schumer, R., Benson, D. A., Meerschaert, M. M., and Baeumer, B.: Fractal mobile/immobile solute transport, *Water Resour. Res.*, 39, 1296, doi:10.1029/2003WR002141, 2003.

5 Selim, H. M. and Ma, L.: Transport of reactive solutes in soils: a modified two region approach, *Soil Sci. Soc. Am. J.*, 59, 75–82, 1995.

Valocchi, A. J.: Validity of the local equilibrium assumption for modeling sorbing solute transport through homogeneous soils, *Water Resour. Res.*, 21, 808–820, 1985.

10 Van Genuchten, M. T. and Wierenga, J.: Mass transfer studies in sorbing porous media, I – Analytical solutions, *SSSA Proceedings*, 40, 473–480, 1976.

Wang, Q., Zhan, H., and Tang, Z.: Forchheimer flow to a well considering time-dependent critical radius, *Hydrol. Earth Syst. Sci. Discuss.*, 10, 14095–14129, doi:10.5194/hessd-10-14095-2013, 2013.

15 Zafarani, A. and Detwiler, R. L.: An efficient time-domain approach for simulating Pe-dependent transport through fracture intersections, *Adv. Water Resour.*, 53, 198–207, 2013.

Zhang, Z. and Nemcik, J.: Fluid flow regimes and nonlinear flow characteristics in deformable rock fractures, *J. Hydrol.*, 477, 139–151, 2013.

On the reliability of analytical models to predict solute transport

C. Cherubini et al.

Table 1. Estimated values of parameters, root mean square error RMSE and determination coefficient r^2 for mobile–immobile model MIM at different injection flow rates in the fractured medium.

MIM 1 no.	Q_0 ($\text{m}^3 \text{s}^{-1}$) $\times 10^{-6}$	v/L (s^{-1}) $\times 10^{-2}$	D/L^2 (s^{-1}) $\times 10^{-2}$	α (s^{-1})	β (–)	RMSE	r^2
1	1.3194	0.73 ± 0.0453	0.15 ± 0.0103	0.004 ± 0.0009	0.95 ± 0.1442	0.0220	0.9786
5	2.2090	1.05 ± 0.0482	0.16 ± 0.0096	0.005 ± 0.0012	0.51 ± 0.0705	0.0213	0.9915
10	2.7312	1.26 ± 0.0478	0.18 ± 0.0095	0.006 ± 0.0012	0.51 ± 0.0596	0.0212	0.9938
15	3.0842	1.74 ± 0.0580	0.19 ± 0.0105	0.010 ± 0.0016	0.56 ± 0.0526	0.0233	0.9950
20	3.3648	1.75 ± 0.0594	0.20 ± 0.0104	0.011 ± 0.0017	0.54 ± 0.0511	0.0220	0.9956
25	3.6813	2.49 ± 0.1037	0.25 ± 0.0166	0.017 ± 0.0032	0.51 ± 0.0587	0.0304	0.9948
30	4.0735	2.57 ± 0.1127	0.26 ± 0.0182	0.017 ± 0.0035	0.50 ± 0.0617	0.0333	0.9940
35	4.5356	2.25 ± 0.0942	0.21 ± 0.0153	0.016 ± 0.0029	0.57 ± 0.0626	0.0310	0.9936
40	5.3824	3.20 ± 0.1334	0.26 ± 0.0199	0.027 ± 0.0044	0.61 ± 0.0627	0.0349	0.9944
45	5.8945	3.32 ± 0.1455	0.26 ± 0.0208	0.028 ± 0.0050	0.57 ± 0.0634	0.0358	0.9946
50	6.1684	3.02 ± 0.1478	0.26 ± 0.0205	0.025 ± 0.0052	0.51 ± 0.0673	0.0312	0.9955
55	8.3455	3.54 ± 0.2916	0.35 ± 0.0363	0.030 ± 0.0107	0.41 ± 0.1060	0.0376	0.9948

Title Page

Abstract

Introduction

Conclusions

References

Tables

Figures

⏪

⏩

◀

▶

Back

Close

Full Screen / Esc

Printer-friendly Version

Interactive Discussion

On the reliability of analytical models to predict solute transport

C. Cherubini et al.

Table 2. Estimated values of parameters, root mean square error RMSE and determination coefficient r^2 for ENM2 at different injection flow rates in the fractured medium.

ENM2 no.	Q_0 ($\text{m}^3 \text{s}^{-1}$) $\times 10^{-6}$	A_{eq} (m^2) $\times 10^{-2}$	α_L (m)	RMSE	r^2
1	1.3194	0.031 ± 0.0014	0.1925 ± 0.0863	0.0328	0.9524
5	2.2090	0.032 ± 0.0004	0.0984 ± 0.0064	0.0199	0.9925
10	2.7312	0.033 ± 0.0004	0.0918 ± 0.0048	0.0191	0.9950
15	3.0842	0.028 ± 0.0003	0.0793 ± 0.0033	0.0204	0.9962
20	3.3648	0.031 ± 0.0003	0.0792 ± 0.0029	0.0193	0.9966
25	3.6813	0.024 ± 0.0002	0.0739 ± 0.0030	0.0262	0.9961
30	4.0735	0.025 ± 0.0002	0.0746 ± 0.0032	0.0272	0.9960
35	4.5356	0.033 ± 0.0004	0.0735 ± 0.0035	0.0278	0.9948
40	5.3824	0.028 ± 0.0002	0.0753 ± 0.0020	0.0226	0.9977
45	5.8945	0.029 ± 0.0002	0.0688 ± 0.0017	0.0266	0.9970
50	6.1684	0.033 ± 0.0004	0.0684 ± 0.0018	0.0317	0.9954
55	8.3455	0.036 ± 0.0005	0.0775 ± 0.0020	0.0413	0.9938

[Title Page](#)
[Abstract](#)
[Introduction](#)
[Conclusions](#)
[References](#)
[Tables](#)
[Figures](#)
[⏪](#)
[⏩](#)
[◀](#)
[▶](#)
[Back](#)
[Close](#)
[Full Screen / Esc](#)
[Printer-friendly Version](#)
[Interactive Discussion](#)

On the reliability of analytical models to predict solute transport

C. Cherubini et al.

Table 3. Estimated values of parameters, root mean square error RMSE and determination coefficient r^2 for ENM3 at different injection flow rates in the fractured medium.

ENM3 no	Q_0 ($\text{m}^3 \text{s}^{-1}$) $\times 10^{-6}$	A_{eq} (m^2) $\times 10^{-2}$	α_L (m)	P_Q/P_C (-)	RMSE	r^2
1	1.3194	0.0343 ± 0.0128	0.1925 ± 0.0863	0.8153 ± 0.1717	0.0323	0.9539
5	2.2090	0.0318 ± 0.0011	0.0984 ± 0.0064	0.7558 ± 0.0214	0.0199	0.9925
10	2.7312	0.0328 ± 0.0009	0.0918 ± 0.0048	0.7542 ± 0.0165	0.0190	0.9950
15	3.0842	0.0273 ± 0.0005	0.0793 ± 0.0033	0.7334 ± 0.0119	0.0193	0.9966
20	3.3648	0.0294 ± 0.0005	0.0792 ± 0.0029	0.7239 ± 0.0106	0.0175	0.9972
25	3.6813	0.0222 ± 0.0004	0.0739 ± 0.0030	0.7063 ± 0.0106	0.0228	0.9971
30	4.0735	0.0237 ± 0.0004	0.0746 ± 0.0032	0.7111 ± 0.0115	0.0248	0.9967
35	4.5356	0.0313 ± 0.0006	0.0735 ± 0.0035	0.7124 ± 0.0128	0.0259	0.9955
40	5.3824	0.0261 ± 0.0003	0.0753 ± 0.0020	0.6988 ± 0.0070	0.0164	0.9988
45	5.8945	0.0270 ± 0.0003	0.0688 ± 0.0017	0.6813 ± 0.0060	0.0164	0.9989
50	6.1684	0.0298 ± 0.0003	0.0684 ± 0.0018	0.6614 ± 0.0059	0.0169	0.9987
55	8.3455	0.0313 ± 0.0002	0.0775 ± 0.0020	0.6297 ± 0.0051	0.0161	0.9991

[Title Page](#)
[Abstract](#)
[Introduction](#)
[Conclusions](#)
[References](#)
[Tables](#)
[Figures](#)
[⏪](#)
[⏩](#)
[◀](#)
[▶](#)
[Back](#)
[Close](#)
[Full Screen / Esc](#)
[Printer-friendly Version](#)
[Interactive Discussion](#)


HESSD

10, 14905–14948, 2013

On the reliability of analytical models to predict solute transport

C. Cherubini et al.

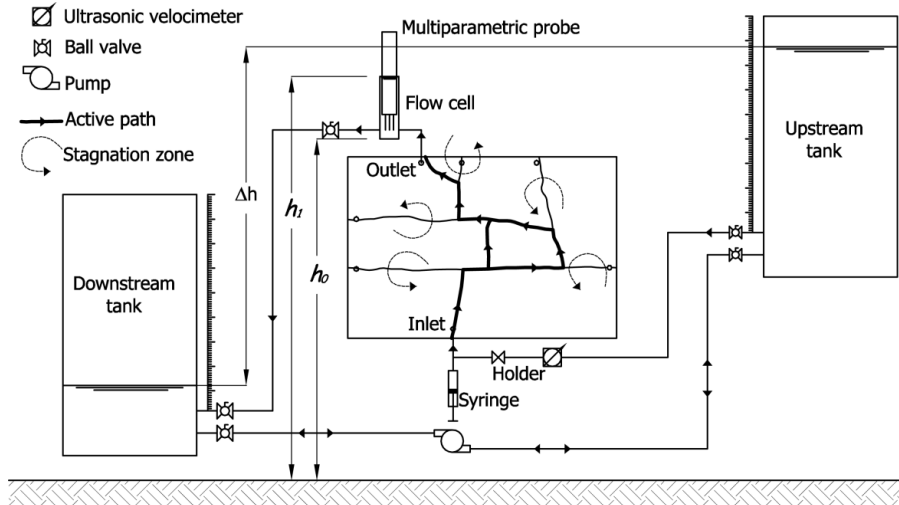


Fig. 1. Schematic diagram of experimental setup.

Title Page	
Abstract	Introduction
Conclusions	References
Tables	Figures
◀	▶
◀	▶
Back	Close
Full Screen / Esc	
Printer-friendly Version	
Interactive Discussion	

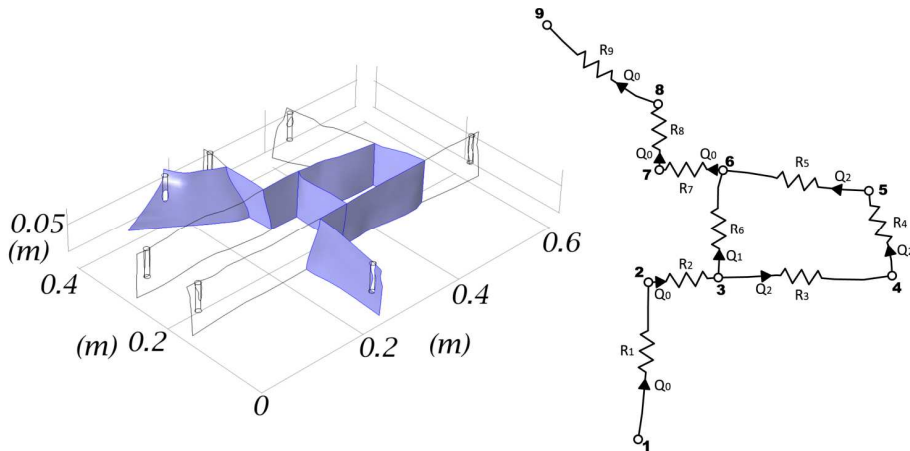


Fig. 2. 2-D pipe network conceptualization of fractured medium.

HESSD

10, 14905–14948, 2013

On the reliability of analytical models to predict solute transport

C. Cherubini et al.

Title Page	
Abstract	Introduction
Conclusions	References
Tables	Figures
◀	▶
◀	▶
Back	Close
Full Screen / Esc	
Printer-friendly Version	
Interactive Discussion	



On the reliability of analytical models to predict solute transport

C. Cherubini et al.

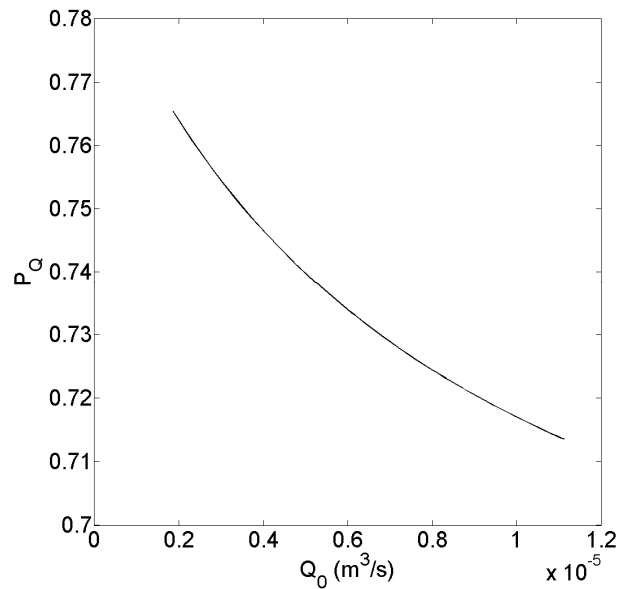


Fig. 4. Probability of water distribution evaluated for main path P_Q vs. injection flow rate Q_0 ($\text{m}^3 \text{s}^{-1}$).

[Title Page](#)[Abstract](#)[Introduction](#)[Conclusions](#)[References](#)[Tables](#)[Figures](#)[⏪](#)[⏩](#)[◀](#)[▶](#)[Back](#)[Close](#)[Full Screen / Esc](#)[Printer-friendly Version](#)[Interactive Discussion](#)

On the reliability of analytical models to predict solute transport

C. Cherubini et al.

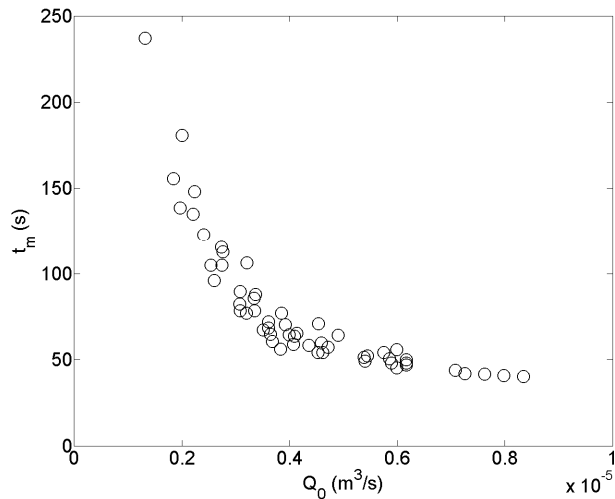


Fig. 5. Mean travel time t_m (s) vs. injection flow rate Q_0 ($\text{m}^3 \text{s}^{-1}$).

[Title Page](#)[Abstract](#)[Introduction](#)[Conclusions](#)[References](#)[Tables](#)[Figures](#)[⏪](#)[⏩](#)[◀](#)[▶](#)[Back](#)[Close](#)[Full Screen / Esc](#)[Printer-friendly Version](#)[Interactive Discussion](#)

On the reliability of analytical models to predict solute transport

C. Cherubini et al.

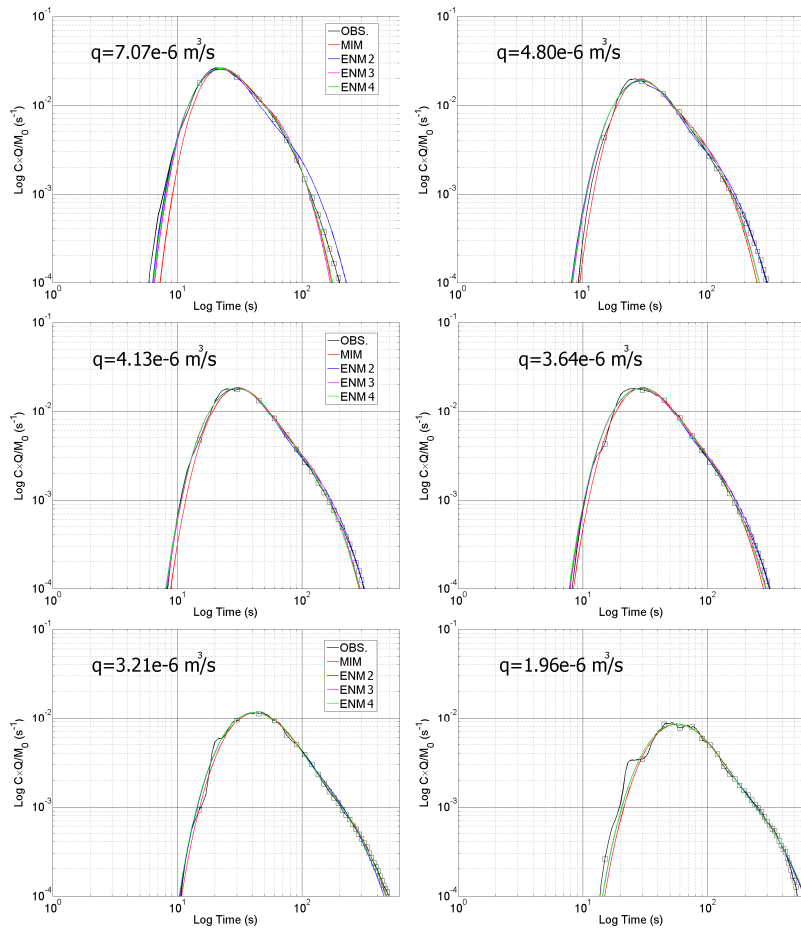


Fig. 6. Fitting of breakthrough curves at different injection flow rates using each of the four models (MIM, ENM1, ENM2, ENM3).

On the reliability of analytical models to predict solute transport

C. Cherubini et al.

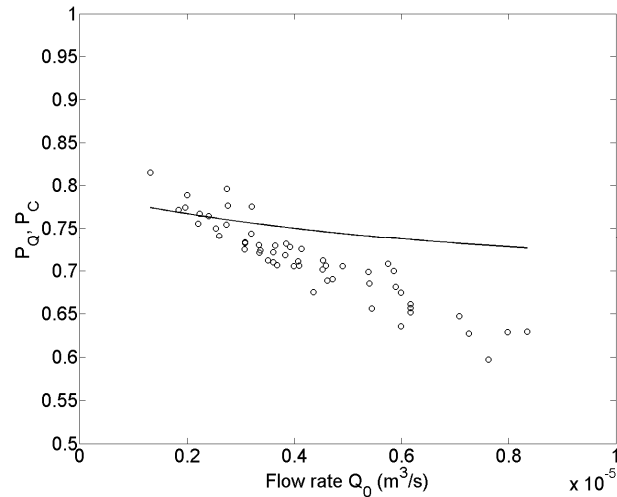


Fig. 7. Comparison between the Probability of water distribution P_Q evaluated by the flow model (straight line) and P_Q supposed equal to the probability of particle transition P_C for ENM3 (circle) varying the injection flow rate Q_0 ($\text{m}^3 \text{s}^{-1}$).

[Title Page](#)[Abstract](#)[Introduction](#)[Conclusions](#)[References](#)[Tables](#)[Figures](#)[⏪](#)[⏩](#)[◀](#)[▶](#)[Back](#)[Close](#)[Full Screen / Esc](#)[Printer-friendly Version](#)[Interactive Discussion](#)

On the reliability of analytical models to predict solute transport

C. Cherubini et al.

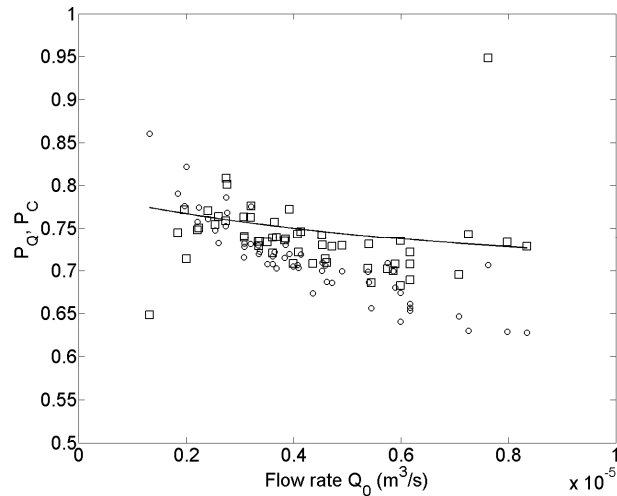


Fig. 8. Comparison between the Probability of water distribution P_Q evaluated by the flow model (straight line) and the probability of particle transition P_C (square) and P_Q (circle) for ENM4 varying the injection flow rate Q_0 ($m^3 s^{-1}$).

[Title Page](#)[Abstract](#)[Introduction](#)[Conclusions](#)[References](#)[Tables](#)[Figures](#)[⏪](#)[⏩](#)[◀](#)[▶](#)[Back](#)[Close](#)[Full Screen / Esc](#)[Printer-friendly Version](#)[Interactive Discussion](#)

On the reliability of analytical models to predict solute transport

C. Cherubini et al.

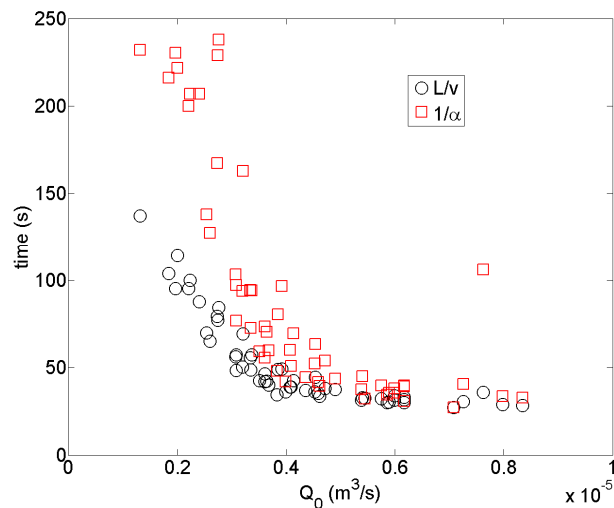


Fig. 9. Transport time (L/v) (reciprocal of normalized velocity) and exchange time ($1/\alpha$) (reciprocal of the exchange term) as function of injection flow rate Q_0 ($m^3 s^{-1}$) for immobile–mobile model MIM.

[Title Page](#)[Abstract](#)[Introduction](#)[Conclusions](#)[References](#)[Tables](#)[Figures](#)[⏪](#)[⏩](#)[◀](#)[▶](#)[Back](#)[Close](#)[Full Screen / Esc](#)[Printer-friendly Version](#)[Interactive Discussion](#)

On the reliability of analytical models to predict solute transport

C. Cherubini et al.

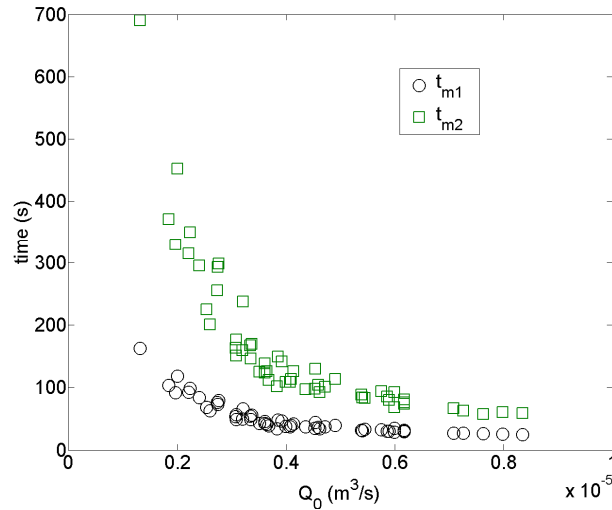


Fig. 10. Travel time for main path t_{m1} (s) and travel time for secondary path t_{m2} (s) for ENM2 as function of injection flow rate Q_0 ($m^3 s^{-1}$).

[Title Page](#)[Abstract](#)[Introduction](#)[Conclusions](#)[References](#)[Tables](#)[Figures](#)[⏪](#)[⏩](#)[◀](#)[▶](#)[Back](#)[Close](#)[Full Screen / Esc](#)[Printer-friendly Version](#)[Interactive Discussion](#)

On the reliability of analytical models to predict solute transport

C. Cherubini et al.

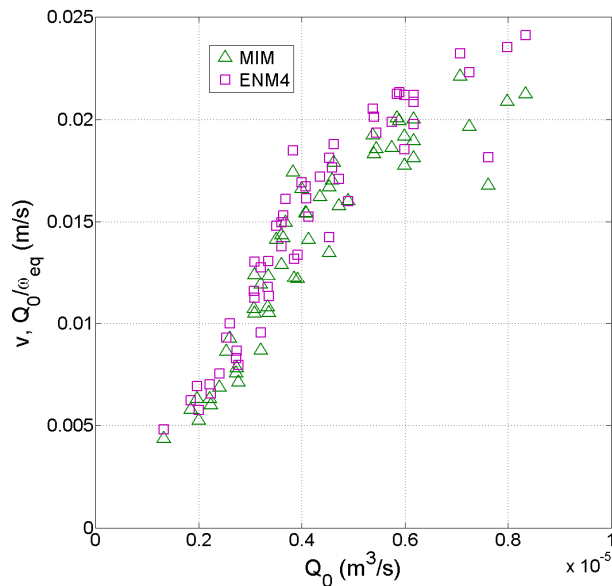


Fig. 11. Velocity v (m s^{-1}) as function of the injection flow rate Q_0 ($\text{m}^3 \text{s}^{-1}$) for MIM and ENM4 models. Note that for MIM model the v is determined assuming the length of medium equal to the length of main path ($L = 0.601$ m). Instead for the ENM4 model the velocity is determined dividing Q_0 for the equivalent area ω_{eq} .

[Title Page](#)
[Abstract](#)
[Introduction](#)
[Conclusions](#)
[References](#)
[Tables](#)
[Figures](#)
[◀](#)
[▶](#)
[◀](#)
[▶](#)
[Back](#)
[Close](#)
[Full Screen / Esc](#)
[Printer-friendly Version](#)
[Interactive Discussion](#)

On the reliability of analytical models to predict solute transport

C. Cherubini et al.

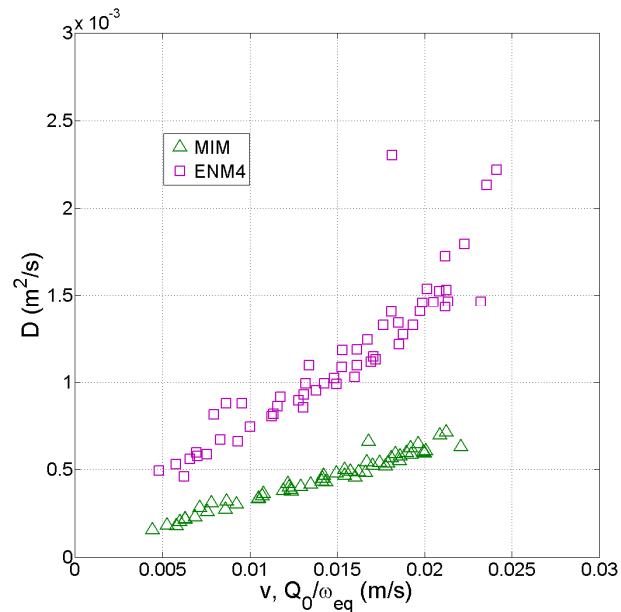


Fig. 12. Dispersion D ($\text{m}^2 \text{s}^{-1}$) as function of velocity for MIM and ENM4 models. Note that for MIM model D is determined assuming the length of the medium equal to the length of the main path ($l = 0.601 \text{ m}$). Instead for ENM4 model D is determined as $D = Q_0 \cdot \alpha_L / \omega_{eq}$.

[Title Page](#)
[Abstract](#)
[Introduction](#)
[Conclusions](#)
[References](#)
[Tables](#)
[Figures](#)
[⏪](#)
[⏩](#)
[◀](#)
[▶](#)
[Back](#)
[Close](#)
[Full Screen / Esc](#)
[Printer-friendly Version](#)
[Interactive Discussion](#)
